Original Article

Annexin A5 involvement in bone overgrowth at the enthesis†

Akemi Shimada,[1]* Hisashi Ideno,[1]* Yoshinori Arai,[2] Koichiro Komatsu,[1] Satoshi Wada,[3] Teruhito Yamashita,[4] Norio Amizuka,[5] Ernst Pöschl,[6] Bent Brachvogel,[7] Yoshiki Nakamura,[3] Kazuhisa Nakashima,[1] Hiroaki Mizukami [8], Yoichi Ezura,[9] Akira Nifuji[1]**

[1] Department of Pharmacology, Tsurumi University School of Dental Medicine, Yokohama, Kanagawa, Japan
[2] Nihon University, School of Dentistry, Chiyoda-ku, Tokyo, Japan
[3] Department of Orthodontics, Tsurumi University School of Dental Medicine, Yokohama, Kanagawa, Japan
[4] Division of Hard Tissue Research, Institute for Oral Science, Matsumoto Dental University, Shiojiri, Nagano, Japan
[5] Department of Developmental Biology of Hard Tissue, Division of Oral Health Science, Graduate School of Dental Medicine, Hokkaido University, Sapporo, Hokkaido, Japan
[6] School of Biological Sciences, University of East Anglia, Norwich Research Park, Norwich, UK
[7] Experimental Neonatology, Department of Pediatrics and Adolescent Medicine, Center for Biochemistry, Medical Faculty, University of Cologne, Cologne, Germany
[8] Division of Genetics Therapeutics, Center for Molecular Medicine, Jichi Medical University, Shimotsuke, Tochigi, Japan.
[9] Department of Molecular Pharmacology, Medical Research Institute, Tokyo Medical and Dental University, Bunkyo-ku, Tokyo, Japan

* Both authors (AS and HI) contributed equally to this study

Corresponding author:

[**]Akira Nifuji DDS, PhD, 2-1-3 Tsurumi, Tsurumi-ku, Yokohama 230-8501, Japan

Tel: +81-45-581-1001, Fax: +81-45-573-9599, E-mail: nifuji-a@tsurumi-u.ac.jp

†This article has been accepted for publication and undergone full peer review but has not been through the copyediting, typesetting, pagination and proofreading process, which may lead to differences between this version and the Version of Record. Please cite this article as doi: [10.1002/jbmr.3453]

Additional Supporting Information may be found in the online version of this article.

Initial Date Submitted August 24, 2017; Date Revision Submitted April 8, 2018; Date Final Disposition Set April 12, 2018

Journal of Bone and Mineral Research

DOI 10.1002/jbmr.3453

Disclosure

All authors state that they have no conflicts of interest.

Abstract

Little is known about the molecular mechanisms of enthesis formation in mature animals. Here, we report that annexin A5 (Anxa5) plays a critical role in the regulation of bone ridge outgrowth at the entheses. We found that Anxa5 is highly expressed in the entheses of postnatal and adult mice. In Anxa5-deficient ($Anxa5^{-/-}$) mice, the sizes of bone ridge outgrowths at the entheses of the tibiae and femur were increased after 7 weeks of age. Bone overgrowth was not observed at the fibrous enthesis where the fibrocartilage layer does not exist. More ALP-expressing cells were observed in the fibrocartilage layer in $Anxa5^{-/-}$ mice than in wild-type (WT) mice. Calcein and Alizarin Red double labeling revealed more mineralized areas in $Anxa5^{-/-}$ mice than WT mice. To examine the effects of mechanical forces, we performed tenotomy in which transmission of contractile forces by the tibial muscle was impaired by surgical muscle release. In tenotomized mice, bone overgrowth at the enthesis in $Anxa5^{-/-}$ mice was decreased to a level comparable to that in WT mice at 8 weeks after the operation. The tail-suspended mice also showed a decrease in bone overgrowth to similar levels in $Anxa5^{-/-}$ and WT mice at 8 weeks after hindlimb unloading. These results suggest that bone overgrowth at the enthesis requires mechanical forces. We further examined effects of AnxaA5 gene knockdown (KD) in primary cultures of osteoblasts, chondrocytes, and tenocytes *in vitro*. AnxaA5 KD increased *ALP* expression in tenocytes and chondrocytes but not in osteoblasts, suggesting that increased ALP activity in the fibrocartilaginous tissue in AnxaA5 KO mice is directly caused by Anxa5 deletion in tenocytes or fibrocartilage cells. These data indicate that Anxa5 prevents bone overgrowth at the enthesis, whose formation is mediated through mechanical forces and modulating expression of mineralization regulators.

Key Words: Annexin A5; lacZ knock-in mouse; enthesis; tendon/ligament; bone morphogenesis

This article is protected by copyright. All rights reserved

Introduction

Tendons and ligaments are connected to bones through a specialized transitional tissue called the enthesis[1,2]. Various types of enthesopathies can cause serious clinical symptoms and their prevalence is increasing in aging societies; thus, it is important to unveil the molecular mechanisms controlling enthesis development and maturation[3–7]. Entheses are classified into fibrous and fibrocartilaginous types. At fibrous entheses, the tendons and ligaments are attached either directly or indirectly through the periosteum to the bone, whereas fibrocartilaginous entheses consist of tendon, fibrocartilage, mineralized fibrocartilage, and bone. Fibrocartilage expresses collagen type I and II, whereas mineralized fibrocartilage expresses collagen type II and X. These collagens may function to minimize stress and strain between tendon and bone.

It has been shown that progenitor cells in the enthesis are specified separately from chondroprogenitors. Cell pools derived from Sox9-positive, Scx-positive, and Col1-negative cells form the bone eminences at the enthesis[6]. TGFβ signaling controls the specification of bone eminence progenitors in the enthesis, and BMP4 signaling regulates their differentiation[8]. GDF5-expressing progenitors contribute to enthesis and tendon formation[9]. Enthesis fibrocartilage cells are also derived from a certain population of Gli-expressing Hedgehog (Hh)-responsive cells in the enthesis. Proper Hh signaling is required for enthesis growth and mineralization[4,9]. It was also previously suggested that muscle-induced mechanical loading plays a role in the growth and mineralization of fibrocartilaginous enthesis[3,4]. Thus far, however, little is known about the molecular mechanisms by which fibrocartilage or other cells respond to mechanical stimuli to develop and maintain the enthesis.

Annexins are soluble proteins and are recruited to membranes containing negatively charged phospholipids in the presence of Ca^{2+}[10–12]. Among them, annexin A5

(Anxa5) was originally isolated from chondrocytes and characterized as a collagen-binding glycoprotein. Anxa5 mediates the Ca^{2+} influx into matrix vesicles secreted from hypertrophic chondrocytes in the growth plate by interacting with extracellular type II and type X collagens, thereby initiating cartilage calcification[13]. Anxa5 participates in plugging the pores in the disrupted cell membrane in the stress-induced condition. The *Anxa5* gene is expressed in the developing cartilage anlagen in vertebral bodies, ribs, and the limb digits[14]. Our previous study indicated that Anxa5 was strongly expressed in mature animal tissues that respond to mechanical stimuli including the periosteum, periodontal ligament, and entheses[15]. Although skeletal development and *in vitro* calcification of isolated chondrocytes are not impaired in Anxa5-deficient ($Anxa5^{-/-}$) mice[16], it is still possible that Anxa5 plays roles in the maintenance of load-bearing transitional tissue.

Therefore, in the present study, we investigated the functions of Anxa5 in the musculoskeletal system in mature animals using $Anxa5^{-/-}$ mice. We found that $Anxa5^{-/-}$ mice show bone ridge overgrowth at the enthesis, and that Anxa5 may prevent such overgrowth via mechanical forces brought by muscle loading.

Materials and Methods

Mice

All animal experiments were approved by the Institutional Animal Care Committee and the Recombination Experiment and Biosafety Committee of Tsurumi University School of Dental Medicine. Mice were kept under specific-pathogen-free (SPF) conditions and fed sterilized CE-2 pellets (CLEA, Tokyo, Japan) and tap water ad libitum. Homozygous mutant ($Anxa5^{-/-}$) and wild-type ($Anxa5^{+/+}$) mice were generated by intercrossing of heterozygous Anxa5-LacZ mice ($Anxa5^{+/-}$)[14,16], which are *Anxa5* null mutants generated by insertion of an in-frame knocked-in LacZ gene. The numbers of mice used are summarized in Table1and

2. To confirm the genotypes, genomic DNA was extracted from the tail tip by standard methods and analyzed by PCR using the following sets of primers for detecting the wild-type (Anxa5Ex4dw: 5´-GAAGCAATGCTCAGCGCCAGGA-3´; Anxa5intron4up: 5´-CCTGTACTCTATCACTATCACTGACTGTTAATC-3´) and the mutant allele (Anxa5Ex3dw: 5´-CGAGAGGCACTGTGACTGACTTCCCTGGAT-3´; LacZ2up: 5´-GCCAGTTTGAGGGGACGACGACAG-3´) as described previously[16]. Mice were sacrificed by cervical dislocation. Body weight and longitudinal tibial length were measured in each genotype and age group. Statistical analyses were performed using two-way ANOVA and Student's *t*-test.

Anxa5-lacZ activity staining

Tissues dissected at 40 weeks of age were fixed with acetone[15] and washed with β-gal reaction buffer consisting of 100 mM sodium phosphate buffer (pH 7.3), 2 mM magnesium chloride, 0.02% Nonidet P-40, and 0.01% sodium deoxycholate. Then, the tissues were stained for β-gal activity by reaction buffer added 1 mg/ml 5-bromo-4-chloro-3-indolyl-β-D-galactoside (X-gal), 5 mM potassium ferricyanide, 5 mM potassium ferrocyanide, and 20 mM Tris-hydrochloric acid (pH 7.3). After staining, the tissues were post-fixed in 4% paraformaldehyde (PFA) in PBS for 24 h at 4 °C and demineralized with 20% EDTA for a month. Part of the demineralized specimens were dehydrated in graded ethanol, cleared in Tissue-Tek® Tissue-Clear™ (Sakura Finetek Japan, Tokyo, Japan), and embedded in Tissue-Tek® Xpress® Paraffin Wax II60 (Sakura Finetek Japan). The remainder of the demineralized specimens were embedded in Tissue-Tek® O.C.T. Compound (Sakura Finetek Japan) using liquid N_2. Paraffinized sections with a thickness of 6 μm were stained with hematoxylin and mounted in MP-500 (Matsunami, Osaka, Japan). Cryosections with a thickness of 14 μm were mounted in Immu-Mount™ (Thermo Shandon,

Cheshire, UK). Specimens were photographed using a digital camera (DP71, Olympus, Tokyo, Japan) connected to a differential interference microscope (Eclipse 80i, Nikon, Tokyo, Japan). Stained whole tissues were photographed with a digital camera connected to a stereomicroscope (MZFLIII, Leica Microsystems Japan, Tokyo, Japan).

Micro-(μ)CT and three-dimensional (3D) reconstruction of μCT images

Tibial, femoral, and mandibular bones were dissected and fixed with 10% formalin in PBS. The bones were scanned at 90 kV, 90 μA, 10 μm/pixel with an *in vivo* micro X-ray CT system R_mCT2 (RIGAKU, Tokyo, Japan). 3D and vertical images were reconstructed with i-VIEW type R (J. MORITA MFG. CORP., Kyoto, Japan).

Peripheral quantitative (pQ)CT

The Latheta LCT-100 Lite (Aloka, Tokyo, Japan) with software 2.10 (Aloka, Tokyo, Japan) was used to analyze cross-sectional areas of cortical bone (Ct.CSA, mm^2). Right or left whole tibial and femoral bones were dissected, fixed with 10% formalin in PBS, and scanned at a pixel size of 70 × 70 μm and a slice thickness of 90 μm. The mean Ct.CSA values of 80 and 100 slices of 90 μm thickness from the proximal end to the epiphysial region of tibial and femoral bones, respectively, were calculated.

Histological analyses

Bones collected at 40 weeks of age were fixed with 4% PFA in PBS, decalcified with 20% EDTA, and embedded in O.C.T. coumpound. Cryosections (14 μm thick) were prepared for hematoxylin-eosin (HE) staining. Immunohistochemistry of Anxa5, and pSMAD1/5/8 were carried out using anti-human Annexin V antibody (1:100, BioVision, CA, USA), anti-phospho SMAD1/5/8 (Ser463/465) antibody (1:100, Millipore, CA, USA), Alexa

Fluor® 594-conjugated chicken anti-rabbit IgG (Thermo Fisher Scientific, MA, USA) and Alexa Fluor® 488-conjugated goat anti-rabbit IgG (Thermo Fisher Scientific), and the sections were counterstained with 4',6-diamidino-2-phenylindole (DAPI). Alkaline phophatase (ALP) and tartrate-resistant alkaline phosphatase (TRAP) activities as markers of bone formation and bone resorption, respectively, were detected by staining assay as previously described[17].

Histomorphometric analysis of bone

Histomorphometric analysis was performed as described previously(ref). Briefly, calcein (4 mg/kg body weight) and Alizarin Red S (20 mg/kg body weight) were injected subcutaneously 13 and 2 days before sacrifice, respectively. Tibiae were embedded in methyl methacrylate, and approximately 100-mm-thick horizontal sections of distal metaphyses and midshaft regions were prepared. Calcein and alizarin red labeling was visualized using a fluorescence microscope (Eclipse 80i, Nikon, Japan) with an excitation wavelength of 450-490 nm and a 510-560 nm band-pass filter, respectively. Mineral apposition rate (MAR) was calculated as the distance between the two labels divided by the time between dye injections[18]. Two-dimensional cortical periosteal perimeter (Ct.Pm) on the bone surface were measured based on cross-sectional slice images captured from μCT (Supplemental Fig.2)

Tendon-severing operation (tenotomy)

Under anesthesia by intraperitoneal injection of pentobarbital (55 mg/kg body weight), the right patellar and tibialis anterior tendons of 12-week-old Anxa5$^{-/-}$ (*n*=4) and Anxa5$^{+/+}$ (*n*=5) mice were severed with a scalpel. The left tibial bones were used as a normal

control. After 8 weeks, tibiae were dissected and histologically and radiographically analyzed by μCT and pQCT. The numbers of mice used are summarized in Table 2.

Hindlimb unloading in tail-suspended mice

The mice were subjected to tail suspension as described previously[19]. Briefly, a 0.3-mm steel wire was applied to the intervertebral space 1-cm from the base of the tail and shaped into a ring from which the mice were suspended. One end of an S-shaped steel wire was placed into the ring and the other end was fixed to the overhead bar and the height of the bar was adjusted to maintain in an 30° head-down tilt with the hindlimbs elevated above the floor of the cage. Mice were permitted to move within the cage using their forelimbs while their hindlimbs were kept free of weight bearing. The mice in the unloading group were subjected to tail suspension for 8 weeks. Loaded control mice were also housed individually under the same conditions except for tail suspension for 8 weeks. After 8 weeks of tail suspension, the femora and tibiae were separated from adherent muscles and connective tissues other than periosteum, and fixed with 70% ethyl alcohol solution for subsequent analysis of bone. The numbers of mice used are summarized in Table 2.

Culture of primary cells

Primary osteoblasts (pOb), primary tenocytes (pTeno), and primary chondrocytes (pCh) were prepared as previoulsy described[20–22] and maintained in growth medium (pOb and pTeno: alpha-MEM (Sigma) supplemented with 10% fetal bovine serum, pCh: DMEM (Gibco) supplemented with 10% fetal bovine serum) in a humidified atmosphere of 5% CO_2 and 95% air.

To induce differentiation, the medium was changed to differentiation medium (pOb: 50 μg/ml ascorbic acid and 10 mM β-glycerophosphate; pTeno: 20 ng/ml Tgf-β2; pCh: 500

ng/ml BMP, 10 ng/ml Tgf-β3, 50 μg/ml ascorbic acid, 10-7M dexamethasone, 40 μg/ml proline, 100 μg/ml pyruvate and 1x ITS-plus) at 1 day after cell seeding and siRNA transfection.

Transfection of siRNA

For the siRNA experiment, we selected a synthetic siRNA duplex against Anxa5 (Anxa5-MSS202025) from Stealth Designer (Life Technologies Japan). Stealth RNAi siRNA Negative Control Lo GC was used as a negative control. To transfect siRNAs, each cell type was seeded at 2×10^4 cells/cm^2 in 6-well plates for 30 min before transfection. The cells were transfected with Anxa5 siRNA or negative control siRNA at a final concentration of 30 nM using jetPRIME transfection reagent (Polyplus Transfection, Illkirch, France).

RNA extraction and quantitative (q) PCR

At 3 days after changing to differentiation medium, RNA was isolated according to the manufacturer's instructions using an RNeasy mini kit (Qiagen, Hilden, Germany). RNA was then reverse-transcribed using oligo-dT primers and reverse transcriptase (Superscript III; Invitrogen) to synthesize cDNA. After cDNA synthesis, qPCR was performed as described[22]. Primer sequences used for qPCR analysis are summarized in Table 3.

Results

Anxa5 is expressed in the skeletal system

We first examined if the Anxa5 is expressed in the enthesis, periosteum, and skeletal tissue by utilizing the LacZ staining of the bones derived from *Anxa5*$^{+/-}$ mice. Anxa5-lacZ was expressed in the enthesis, periosteum, articular cartilage surface, and growth plate cartilage of the tibial bone in Anxa5$^{+/-}$ mice (Fig. 1A–C). In magnified views of insertion sites of the soleus muscle to the medial surface of the tibia, Anxa5-lacZ expression was observed in fibrocartilaginous tissues (Fig. 1D). Similar expression patterns of Anxa5-lacZ were observed in femoral bones (data not shown). Expression of Anxa5-lacZ was also observed at insertion sites of the masseter and digastric muscles to the mandibular bone, and those of the periodontal ligament to the alveolar bone (Fig. 1E–G). The localization of Anxa5 protein in fibrocartilaginous tissues as determined by histochemical staining was similar to that of Anxa5-lacZ (Fig. 1D and H).

Bone ridge overgrowth at the entheses of Anxa5$^{-/-}$ mice

We next examined the skeletal phenotype of the Anxa5-/- mice. Consistent with previous study, the Anxa5$^{-/-}$ mice were viable and fertile, and showed no significant differences in body weight and longitudinal tibial bone length until 40 weeks of age when compared to Anxa5$^{+/+}$ and Anxa5$^{+/-}$ mice (Supplemental Fig. 1). However, under a binocular microscope, we found that several portions of tendon insertions to the bones were projected abnormally in the *Anxa5*$^{-/-}$ mice compared to the wild-type mice. For example, the bone ridge at the insertion of the tibialis anterior muscle (Fig. 2A), and that at the trochanter tertius of the proximal femur was prominent in the *Anxa5*$^{-/-}$ mice (Fig. 3A).

At 40 weeks of age, microscopic observation revealed that tibial bone ridge overgrowth was prominent in Anxa5$^{-/-}$ mice and that the bone ridge size in Anxa5$^{+/-}$ mice was

intermediate between those in Anxa5$^{-/-}$ and Anxa5$^{+/+}$ mice (Fig. 2A and supplemental Fig. 3A). In accordance with the microscopic view, μCT analysis and measurement of Cortical periosteal perimeter (Ct.Pm) showed that the largest the Ct.CSA and Ct.Pm at the level of tibial bone ridge in Anxa5$^{-/-}$ mice and those in Anxa5$^{+/-}$ mice were intermediate between those in Anxa5$^{-/-}$ and Anxa5$^{+/+}$ mice (Fig. 2B). These changes of bone ridge overgrowth were apparent after 7 weeks, but not before 4 weeks of age (Fig. 2C and D). Similarly, microscopic and μCT analyses revealed that the femoral and mandibular bone showed bone ridge overgrowth at the entheses (Fig. 3, and supplemental Fig. 3B, C). In contrast to these fibrocartilaginous entheses, the fibrous insertions of the ligaments were not affected in Anxa5–/– mice. For example, the tibial insertion of the medical collateral ligament with minimal Anxa5-LacZ expression was indistinguishable from that of WT mice (Fig. 4A, B,and C).

Tendon resection and hindlimb unloading suppresses the skeletal phenotype of Anxa5$^{-/-}$ mice

Anxa5$^{-/-}$ mice showed bone ridge overgrowth at the entheses as of 7 weeks of age. To assess whether the localized phenotype at the entheses is caused by changes in the genetically regulated pattern formation of bone outlines or involves mechanical force-driven local growth of fibrocartilaginous tissues, we used tenotomy to eliminate tibial muscle contractile force transmission (Supplemental Fig. 4). Microscopic observation revealed that bone ridge overgrowth at the enthesis was suppressed at tenotomized sites to a similar extent in Anxa5$^{-/-}$ and Anxa5$^{+/+}$ mice (Fig. 5A). μCT analysis supported these findings (Fig. 5A). The increased Ct.CSA and wider fibrocartilaginous layers at the enthesis of Anxa5$^{-/-}$ mice were decreased to levels similar to those in Anxa5$^{+/+}$ mice at 8 weeks after tenotomy (Fig. 5B, C). In contrast, bone ridge overgrowth at the control sites in Anxa5-/- mice was not

altered (Fig. 5A). Body weight did not differ between tenotomized and Anxa5$^{-/-}$ and Anxa5$^{+/+}$ mice (Supplemental Fig. 4B). To reduce muscle loading, we further performed hindlimb unloading in tail-suspended mice. In those mice, the sizes of the bone ridges of the tibia and femur were decreased in both Anxa5$^{+/+}$ and Anxa5$^{-/-}$ mice after hindlimb unloading (Fig. 5D). These results suggest that Anxa5 inhibits bone ridge overgrowth at the enthesis, which depends on mechanical loading by muscle contractile forces.

ALP was activated in fibrocartilaginous tissues at the enthesis in Anxa5$^{-/-}$ mice

The fibrocartilaginous layer was wider in Anxa5$^{-/-}$ mice than in Anxa5$^{+/+}$ mice at the insertion sites (Fig. 6A–D). In these tissues, calcein and Alizarin Red labeling showed higher uptake and broader distribution of labeling in Anxa5$^{-/-}$ mice than in Anxa5$^{+/+}$ mice (Fig. 6E, F). Mineral apposition rate showed higher mineral apposition in Anxa5$^{-/-}$ mice (Fig. 6G). Consistent with these results, a broader distribution of cells with high ALP activity was observed in the fibrocartilaginous layer in Anxa5$^{-/-}$ mice (Fig. 6H, I). The proportion of ALP-positive cells was significantly higher in Anxa5$^{-/-}$ mice than in Anxa5 $^{+/+}$ mice (Fig. 6J).

Because ALP is activated by BMP signaling in various tissues, we next examined BMP signaling in the enthesis by immunofluorescent detection of phosphorylated Smad 1/5/8 . We observed many cells positive for phosphorylated Smad 1/5/8 in the region closed to ALP-positive cells in the enthesis in Anxa5 $^{+/+}$ and Anxa5$^{-/-}$ mice (arrowhead in Fig. 6K and L).

To examine whether overgrowth of the bone ridge is caused by decreased osteoclastic activity at the enthesis, we performed TRAP staining. Cells positive for TRAP activity were minimally detected in both Anxa5$^{-/-}$ and Anxa5$^{+/+}$ mice (Supplemental Fig. 5).

These results suggest that Anxa5 regulates matrix accumulation and mineralization of the bone ridges at the enthesis.

AnxaA5 differentially regulate cell differentiation and ALP expression in three types of cells

We next examined the molecular mechanism underlying the phenotypes observed in Anxa5$^{-/-}$ mice. We analyzed the effects of AnxaA5 gene knockdown (KD) in three representative cellular components of the enthesis: osteoblasts, chondrocytes, and tenocytes *in vitro*. Transfection of AnxaA5 siRNA resulted in increased *ALP* expression in primary cultures of tenocytes and chondrocytes but not in osteoblasts (Fig. 7B). AnxaA5KD in chondrocytes resulted in up-regulation of Sox9, whereas it increased Scx and Tnmd expression in tenocytes , suggesting that AnxaA5KD promotes chondrocyte and tenocyte differentiation (Fig. 7H). AnxaA5KD in osteoblasts resulted in decreased Runx2 and osteopontin expression, suggesting that AnxaA5KD inhibits osteoblastic differentiation (Fig. 7H).

To investigate the possible mechanisms underlying the increase of *ALP* mRNA, we examined the expression of BMP4 and Wnt5a, which are positive and negative regulators of ALP, in various cells. *BMP4* expression was increased in Anxa5 KD osteoblasts and chondrocytes but not in tenocytes (Fig. 7C). In contrast, *Wnt5a* expression was suppressed in Anxa5 KD tenocytes and chondrocytes but not in osteoblasts (Fig. 7D). These findings suggest that increased BMP4 expression and decreased Wnt5a expression may mediate up-regulation of ALP in chondrocytes. Since Hh signaling is important for mineralization in enthesis, we examined Ptc1 expression, which is a target of Hh signaling. *Ptc1* expression was increased in Anxa5 KD chondrocytes but not in tenocytes and osteoblasts (Fig. 7E).

Because ALP has been reported to hydrolyze pyrophosphate (PPi), a potent inhibitor of biomineralization, we examined the expression of enzymes involved in pyrophosphate transport and metabolism. Expression of the progressive ankylosis gene (ank, a transporter of PPi) was decreased in tenocytes and chondrocytes but not in osteoblasts upon Anxa5 KD (Fig. 7F). Expression of the ectonucleotide pyrophosphatase/phosphodiesterase (ENPP1), which generates PPi, was suppressed in chondrocytes but increased in tenocytes and osteoblasts by Anxa5 KD (Fig. 7G). These results suggest that ALP, ANK, and ENPP1 were differentially regulated by Anxa5 in three cellular components of the enthesis. Increased ALP and decreased ANK and ENPP1 levels in chondrocytes favor Pi against PPi in the absence of Anxa5.

Discussion

We investigated here the skeletal phenotype of Anxa5-deficient mice, which have been reported to have less prominent skeletal phenotypes at least until the age of 3 months [16,23]. By focusing on the bony eminences or the enthesis of the ligaments or tendons, we could demonstrate that adult Anxa5-deficient mice have larger bone ridges at various entheses of the skeleton. Enlarged bone ridges with strong Anxa5-lacZ expression were observed at least after 7 weeks of age in the long and facial bones of Anxa5–/– mice, suggesting that Anxa5 may function to inhibit bone ridge overgrowth at the entheses during maturation in adolescent to adult mice. To the best of our knowledge, this is the first report that Anxa5 has a protective function to prevent overgrowth of the bone eminences for the tendon/ligament insertions.

Several hypotheses have been proposed for enthesis formation or modeling/remodeling. For example, the importance of BMP4 for the activation of chondrogenic differentiation of enthesis tendon cells has been reported[8]. In our study, we found that BMP4 expression is increased by knocking down Anxa5 in chondrocytes or in osteoblasts, suggesting its possible involvement. In the literature, the importance of parathyroid hormone-related protein (PTHrP) in the induction of remodeling by osteoclasts was also indicated for fibrous insertions of tendons using Scx-Cre and PTHrP floxed mutant mice[7]. However, in our study, we did not detect any apparent changes in the number of osteoclasts distributed around the remodeling enthesis. Thus, we assume that bone ridge overgrowth at the fibrocartilaginous entheses in Anxa5–/– mice was mainly caused by activation of chondrocytes rather than suppression of osteoclasts.

Because it has been reported that the forces applied by muscles and tendons to the enthesis are important for bone ridge formation [3,24,25], we investigated the effects of mechanical unloading using tendon-severing operation or hindlimb unloading in tail-suspended mice. We found that bone eminences in Anxa5–/– mice were reduced to

levels comparable to those in Anxa5+/+ mice by 8 weeks after tenotomy or hindlimb unloading, suggesting that bone eminence formation in response to mechanical tension is restricted by expression of Anxa5. Although the molecular mechanisms by which the Anxa5 suppresses tension-induced bone ridge growth remains unknown, our study using primary cultured chondrocytes and tenocytes identified novel functions of Anxa5 as follows.

First, the cell-type-specific response of chondrocytes, tenocytes, and osteoblasts was demonstrated by primary culture experiments. Because Anxa5 was expressed in the periosteum, fibrocartilage, and adjacent tendon in the adult mouse skeleton, we investigated these cells. *ALP* expression was increased by Anxa5-KD in primary tenocytes and chondrocytes but not in osteoblasts, suggesting its direct contribution to the increased ALP activity in the fibrocartilaginous tissue in AnxaA5 KO mice. We also found one possible mechanism underlying the increase of *ALP* expression in Anxa5 deletion by up-regulation of BMP4, which is known to activate ALP in various tissues[26,27]. Downregulation of Wnt5a in primary chondrocytes may also be responsible, as it has been reported to decrease ALP expression in cultured chondrocytes, enthesis explant, and periodontal ligament (PDL) cells [28,29]. The increased Bmp4 and decreased Wnt5a levels may be due to the enhanced chondrogenic differentiation. We also showed cell-type-specific response that Sox9 expression in chondrocytes and Scx expression in tenocytes was increased by Anxa5 KD, whereas Runx2 expression in osteoblasts was decreased by Anxa5 KD.

ALP is a critical regulator of mineralization, which hydrolyzes pyrophosphate, a strong inhibitor of extracellular mineralization, into inorganic phosphate (pi)[30]. Importantly, extracellular pyrophosphate is also regulated by another enzyme ENPP[31] and the transporter ANK[32],and thus the observed effects in Anxa5 KD chondrocytes, i.e., the decreased ENPP and ANK expression along with increased ALP expression, was considered to favor mineralization by suppression of extracellular pyrophosphate levels. In addition, if

the enhanced chondrogenic and tenocytic differentiation contributed to the enhanced mineralization at the enthesis, such cell-type-specific control of differentiation may contribute *in vivo* to restrict the skeletal phenotypes of Anxa5–/– mice only to fibrocartilaginous enthesis in adulthood. Anxa5 may function to modify physiological responses *in vivo* such as stress loading condition.

In conclusion, Anxa5 prevents bone overgrowth at the enthesis, whose formation is mediated through mechanical forces and modulating expression of pyrophosphate (PPi) regulators (Fig. 8). Further studies are needed to clarify the molecular mechanisms of Anxa5 fuctions in the enthesis. An in-depth understanding of Anxa5 functions may shed light on the mechanism of pathologic condition of the human entheses.

Acknowledgement

The present study was supported by JSPS KAKENHI Grant Numbers 21659425, 23659862, 15K15679 to AN , 22592053, 26462825 to AS, and 26861562, 17K18196 to HI.

Authors' roles: Study design: AN, KN, and YE. Conduct experiment: AS, HI, YA, KN, KK, SW, and HM. Mouse model generation: EP and BB. Data collection: AS, HI,YA, KK, SW, TY and KN. Data analysis: AS,HI, YA, and AN. Data interpretation: AS, HI,NA, YN, KN, YE, and AN. Drafting manuscript: AS,YE, KN and AN. AN takes responsibility for the integrity of the data analysis.

References

1. Thomopoulos S, Genin GM, Galatz LM. The development and morphogenesis of the tendon-to-bone insertion - What development can teach us about healing. J. Musculoskelet. Neuronal Interact. 2010;10(1):35–45.
2. Benjamin M, Toumi H, Ralphs JR, Bydder G, Best TM, Milz S. Where tendons and ligaments meet bone: Attachment sites ('entheses') in relation to exercise and/or mechanical load. J. Anat. 2006;208(4):471–90.
3. Schwartz AG, Lipner JH, Pasteris JD, Genin GM, Thomopoulos S. Muscle loading is necessary for the formation of a functional tendon enthesis. Bone. 2013;55(1):44–51.
4. Schwartz AG, Long F, Thomopoulos S. Enthesis fibrocartilage cells originate from a population of Hedgehog-responsive cells modulated by the loading environment. Development. 2015;142(1):196–206.
5. Schwartz AG, Pasteris JD, Genin GM, Daulton TL, Thomopoulos S. Mineral Distributions at the Developing Tendon Enthesis. PLoS One. 2012;7(11).
6. Sugimoto Y, Takimoto A, Akiyama H, Kist R, Scherer G, Nakamura T, Hiraki Y, Shukunami C. Scx+/Sox9+ progenitors contribute to the establishment of the junction between cartilage and tendon/ligament. Development. 2013;140(11):2280–8.
7. Wang M, Vanhouten JN, Nasiri AR, Johnson RL, Broadus AE. PTHrP regulates the modeling of cortical bone surfaces at fibrous insertion sites during growth. J. Bone Miner. Res. 2013;28(3):598–607.
8. Blitz E, Viukov S, Sharir A, Shwartz Y, Galloway JL, Pryce BA, Johnson RL, Tabin CJ, Schweitzer R, Zelzer E. Bone Ridge Patterning during Musculoskeletal Assembly Is Mediated through SCX Regulation of Bmp4 at the Tendon-Skeleton Junction. Dev. Cell. 2009;17(6):861–73.

9. Dyment NA, Breidenbach AP, Schwartz AG, Russell RP, Aschbacher-Smith L, Liu H, Hagiwara Y, Jiang R, Thomopoulos S, Butler DL, Rowe DW. Gdf5 progenitors give rise to fibrocartilage cells that mineralize via hedgehog signaling to form the zonal enthesis. Dev. Biol. 2015;405(1):96–107.

10. Rescher U. Annexins - unique membrane binding proteins with diverse functions. J. Cell Sci. 2004;117(13):2631–9.

11. Gerke V, Creutz CE, Moss SE. Annexins: Linking Ca2+ signalling to membrane dynamics. Nat. Rev. Mol. Cell Biol. 2005;6(6):449–61.

12. Monastyrskaya K, Babiychuk EB, Draeger A. The annexins: Spatial and temporal coordination of signaling events during cellular stress. Cell. Mol. Life Sci. 2009;66(16):2623–42.

13. Kirsch T, Harrison G, Golub EE, Nah HD. The roles of annexins and types II and X collagen in matrix vesicle-mediated mineralization of growth plate cartilage. J. Biol. Chem. 2000;275(45):35577–83.

14. Brachvogel B, Welzel H, Moch H, Von Der Mark K, Hofmann C, Pöschl E. Sequential expression of annexin A5 in the vasculature and skeletal elements during mouse development. Mech. Dev. 2001;109(2):389–93.

15. Shimada A, Komatsu K, Nakashima K, Pöschl E, Nifuji A. Improved methods for detection of β-galactosidase (lacZ) activity in hard tissue. Histochem. Cell Biol. 2012;137(6):841–7.

16. Brachvogel B, Dikschas J, Moch H, Welzel H, von der Mark K, Hofmann C, Pöschl E. Annexin A5 is not essential for skeletal development. Mol. Cell. Biol. 2003;23(8):2907–13.

17. Komatsu K, Shimada A, Shibata T, Wada S, Ideno H, Nakashima K, Amizuka N, Noda M, Nifuji A. Alendronate promotes bone formation by inhibiting protein prenylation in osteoblasts in rat tooth replantation model. J. Endocrinol. 2013;219(2): 145-158.

18. Dempster DW, Compston JE, Drezner MK, Glorieux FH, Kanis JA, Malluche H, Meunier PJ, Ott SM, Recker RR, Parfitt AM. Standardized nomenclature, symbols, and units for bone histomorphometry: A 2012 update of the report of the ASBMR Histomorphometry Nomenclature Committee. J. Bone Miner. Res. 2013;28(1):2–17.

19. Ishijima M, Tsuji K, Rittling SR, Yamashita T, Kurosawa H, Denhardt DT, Nifuji A, Noda M. Resistance to unloading-induced three-dimensional bone loss in osteopontin-deficient mice. J. Bone Miner. Res. 2002;17(4):661-667.

20. Yagi K, Tsuji K, Nifuji A, Shinomiya K, Nakashima K, DeCrombrugghe B, Noda M. Bone morphogenetic protein-2 enhances osterix gene expression in chondrocytes. J. Cell. Biochem. 2003;88(6):1077–1083.

21. Shimada A, Wada S, Inoue K, Ideno H, Kamiunten T, Komatsu K, Kudo A, Nakamura Y, Sato T, Nakashima K, Nifuji A. Efficient expansion of mouse primary tenocytes using a novel collagen gel culture method. Histochem. Cell Biol. 2014;142(2): 205–215.

22. Ideno H, Takanabe R, Shimada A, Imaizumi K, Araki R, Abe M, Nifuji A. Protein related to DAN and cerberus (PRDC) inhibits osteoblastic differentiation and its suppression promotes osteogenesis in vitro. Exp. Cell Res. 2009;315(3):474–84.

23. Belluoccio D, Grskovic I, Niehoff A, Schlötzer-Schrehardt U, Rosenbaum S, Etich J, Frie C, Pausch F, Moss SE, Pöschl E, Bateman JF, Brachvogel B. Deficiency of annexins A5 and A6 induces complex changes in the transcriptome of growth plate cartilage but does not inhibit the induction of mineralization. J. Bone Miner. Res. 2010;25(1):141–53.

24. Killian ML, Thomopoulos S. Scleraxis is required for the development of a functional tendon enthesis. FASEB J. 2016;30(1):301–11.

25. Thomopoulos S, Kim H-M, Rothermich SY, Biederstadt C, Das R, Galatz LM. Decreased muscle loading delays maturation of the tendon enthesis during postnatal development. J. Orthop. Res. 2007;25(9):1154–63.

26. Rahman MS, Akhtar N, Jamil HM, Banik RS, Asaduzzaman SM. TGF-β/BMP signaling and other molecular events: Regulation of osteoblastogenesis and bone formation. Bone Res. 2015;3(November 2014):15005; doi:10.1038/.

27. Kim YJ, Lee MH, Wozney JM, Cho JY, Ryoo HM. Bone morphogenetic protein-2-induced alkaline phosphatase expression is stimulated by Dlx5 and repressed by Msx2. J. Biol. Chem. 2004;279(49):50773–80.

28. Hasegawa D, Wada N, Yoshida S, Mitarai H, Arima M, Tomokiyo A, Hamano S, Sugii H, Maeda H. Wnt5a Suppresses Osteoblastic Differentiation of Human Periodontal Ligament Stem Cell-like Cells Via Ror2/JNK signaling. J. Cell. Physiol. 2017;233:1752–62.

29. Bougault C, Briolay A, Boutet MA, Pilet P, Delplace S, Le Goff B, Guicheux J, Blanchard F, Magne D. Wnt5a is expressed in spondyloarthritis and exerts opposite effects on enthesis and bone in murine organ and cell cultures. Transl. Res. 2015;166(6):627–38.

30. Orriss IR, Arnett TR, Russell RGG. Pyrophosphate: A key inhibitor of mineralisation. Curr. Opin. Pharmacol. 2016;28:57–68.

31. Mackenzie NCW, Huesa C, Rutsch F, MacRae VE. New insights into NPP1 function: Lessons from clinical and animal studies. Bone. 2012;51(5):961–8.

32. Ho AM, Johnson MD, Kingsley DM. Role of the mouse ank gene in control of tissue calcification and arthritis. Science. 2000;289(5477):265–70.

Figure captions

Fig. 1. Anxa5-lacZ and Anxa5 expression.

(**A**) Anxa5-lacZ expression at tendon insertion sites to the tibial bone in Anxa5$^{+/-}$ male mouse at 40 weeks of age. The leg was dissected out, fixed with acetone, and stained with X-gal. Intensive blue staining (arrowheads) was observed at sites where tendons attach to the bone. The tibialis anterior muscle was eliminated to clearly show the region with strong expression. (**B**) Longitudinal section of tibia showing the presence of the Anxa5-lacZ fusion protein by staining with X-gal and hematoxylin. The blue X-gal staining was observed at insertion sites of tendon/ligament to bone, surface of articular cartilage, growth plate cartilage, and periosteum. (**C**) Transverse section of tibial bone showing the presence of Anxa5-lacZ by X-gal staining. Fdl, flexor digitorum longus muscle; S, soleus muscle; Ta, tibialis anterior muscle; Tp, tibialis posterior muscle. The square indicates the area magnified in (D). (**D**) Anxa5-lacZ expression at tendon insertion sites of the soleus muscle to the tibial bone. Strong expression of Anxa5-lacZ was observed in the enthesis region surrounded by dotted lines in the image. (**E**) Ventral view of mandibles stained for Anxa5-lacZ with X-gal. The blue X-gal staining (arrowheads) was observed at insertion sites of the tendon to the bone. (**F**) Frontal section of mandible stained for Anxa5-lacZ. The blue X-gal staining was observed at the insertion sites of the masseter and digastric muscles to the mandibular bone and periodontal ligaments of the molar and incisor teeth. The square indicates the site magnified in (G). (**G**) Anxa5-lacZ expression at tendon insertion sites of the digastric muscle to the mandibular bone. (**H**) Immunohistochemistry showing Anxa5 expression at the insertion site of the soleus muscle to the tibial bone. Strong expression of Anxa5, similar to Anxa5-lacZ in (D), was observed in the enthesis region (surrounded by dotted lines). Cells were counterstained with DAPI. Dg; digastric muscle, I; incisor, Fdl;

flexor digitorum longus muscle, M3; third molar, Ma; mandibular bone, Mm; masseter muscle, S; soleus muscle, Ta; tibialis anterior muscle, Ti; tibia, Tp; tibialis posterior muscle.

Fig 2. Analyses of tibial bones in Anxa5$^{-/-}$ mice

(**A**) Representative view of microscopic images(upper) , reconstructed μCT images (middle), and cross-sectional images (lower) at insertion sites of tibial bone at 40 weeks of age in female mice. Images of tibia for Anxa5$^{+/+}$ (WT), Anxa5$^{+/-}$ (Het) , and Anxa5$^{-/-}$ (KO) are shown .Bone ridge protrusions are indicated by arrowheads. Scale bar, 1 mm. (**B**) Means of cortical cross-sectional area (Ct.CSA) (left and middle panel) and cortical periosteal perimeter (Ct.Pm) (right panel) of tibial bone at 40 weeks of age in female mice are shown. Squares in the left panel indicate the sites magnified in the middle panel. One star (*) and two stars (**) indicate significant difference of WT and KO with a P value <0 .05 and < 0.01, respectively. Ct.Pm is measured in the cross sectional images of μCT at the position as the distance (in mm) from the growth plate, shown in Supplemental Fig. 2. (**C**) Representative reconstructed 3D image of tibial bones that were dissected at 4, 7, and 16 weeks (W) from female. Scale bars, 1 mm. (**D**) Mean Ct.CSA of tibial bones measured by pQCT. Fixed tibial bones were analyzed by pQCT using 100 slices of 90 μm thickness covering the proximal end to the diaphyseal region. Obvious increases in Ct.CSA in Anxa5$^{-/-}$ mice after 7 weeks of age are indicated by arrowheads.

Fig. 3. Analyses of femoral bones in Anxa5$^{-/-}$ mice.

(**A**) Representative view of microscopic images(upper) , reconstructed 3D μCT images (middle) and cross-sectional images (lower panel) at insertion sites of femoral bone at 16 weeks of age. Bone ridge protrusions at the enthesis of the trochanter tertius in femur are indicated by arrowheads. Scale bar, 1 mm. (**B**) Mean Ct.CSA of femoral bone measured by

pQCT. Mean Ct.CSA of 3 to 5 of Anxa5$^{+/+}$ (WT; *black dotted line*) and Anxa5$^{-/-}$ (KO; *black line*) mice from each age groups are plotted. Increases in Ct.CSA in Anxa5$^{-/-}$ mice after 7 weeks of age are indicated by arrowheads.

Fig. 4. Analyses of fibrous enthesis of tibia.

(A) Anxa5-lacZ expression at fibrous entheses. Anxa5-lacZ expression was hardly observed at the fibrous insertion of the medial collateral ligament (MCL) to the tibial bone (Ti). The dotted line indicates the site used for histological analyses in (C). Scale bar, 100 μm (**B**) Representative view of microscopic images and reconstructed μCT images of tibial bone at 4, 16, and 40 weeks (w) of female mice showed no phenotypic differences between Anxa5$^{+/+}$ (WT) and Anxa5$^{-/-}$ (KO) mice. **(C)** HE staining of transverse sections showing insertion sites of MCL to Ti in Anxa5$^{+/+}$ (WT) and Anxa5$^{-/-}$ mice (KO) at 40 weeks of age. No marked differences were observed between Anxa5$^{+/+}$ and Anxa5$^{-/-}$ mice. Dotted lines delineate tibia (Ti), fibrous tissue, and MCL.

Fig.5. Effect of mechanical unloading on bone ridge overgrowth at the enthesis. (**A**) Representative images of normal (C) and tenotomized (T) sides of tibial bones in Anxa5$^{+/+}$ (WT) and Anxa5$^{-/-}$ (KO) mice. Representative view of microscopic images, reconstructed 3D μCT images and cross sectional images of tibiae are shown. Decreases in bony protrusions in Anxa5$^{-/-}$ and Anxa5$^{+/+}$ mice are indicated by arrowheads. Scale bars, 1 mm. (**B**) Mean Ct.CSA of normal and tenotomized sides of bones of Anxa5$^{+/+}$(WT) and Anxa5$^{-/-}$ (KO) mice. pQCT analyses were conducted as described in the legend of Fig. 2. Decreases in Ct.CSA are indicated by arrowheads. (**C**) HE staining of transverse sections showing insertion sites of the soleus muscle to the tibial bone of the tenotomyzed side. In tenotomized mice, the bone ridge protrusions in Anxa5$^{-/-}$ (KO) mice was suppressed to a

level comparable to that in Anxa5$^{+/+}$(WT) mice. Scale bars, 100 μm. (**D**) Analysis of femur after 8week tail suspension. Tail suspension started at 12 weeks of age and continued for 8 weeks. Representative view of microscopic images of femur at 20 weeks of age in Anxa5$^{+/+}$ (W) loading (L) and unloading (UL) mice, and that in Anxa5$^{-/-}$ (KO) loading (L) and unloading (UL) mice are shown. Bone ridge protrusions at the enthesis of the trochanter tertius in femur are inidacted by arrowheads.

Fig. 6. Histological analyses of tibial bones in Anxa5$^{-/-}$ (KO) and Anxa5$^{+/+}$(WT) mice. (**A, B**) HE staining of transverse sections showing insertion sites of the soleus muscle to the tibial bone in Anxa5$^{+/+}$ (A) and Anxa5$^{-/-}$ (B) mice at 40 weeks of age. Squares indicate the sites magnified in Fig. 6C and D. (**C, D**) Magnified images of HE staining at insertion sites of the soleus muscle to the tibial bone. Anxa5$^{-/-}$ mice (D) showed increased amounts of fibrocartilaginous tissues, surrounded by dotted lines in the image. (**E, F, and G**) Calcein and alizarin red uptake at the insertion sites of the soleus muscle to the tibial bone. MAR were calculated, based on the double labeling (G). MRA was significantly higher in Anxa5$^{-/-}$mice (G; *$p < 0.05$, *t*-test) (**H, I, and J**) Representative images of ALP-expressing cells (I, J) in insertion sites of the soleus muscle to the tibial bone. More ALP-expressing cells with intensive activity were observed in fibrocartilaginous tissues (surrounded by dotted lines) in Anxa5$^{-/-}$ (H) than in those of Anxa5$^{+/+}$ (I) mice. The percentage of ALP-expressing cells in total cells was significantly higher in Anxa5$^{-/-}$mice (J; *$p < 0.05$, *t*-test). (**K, L**) Immunohistochemical analysis of pSmad 1/5/8. Immunofluorescence of pSmad 1/5/8, counterstained by DAPI are shown. Positive cells in are indicated by arrowheads in fibrocartilaginous tissues (surrounded by dotted lines) Anxa5$^{+/+}$ (K) and Anxa5$^{-/-}$ (L) mice. Scale bars, 500 μm (A, B) and 100 μm (C-F, H, I, K, and L). Abbreviations are listed in the legend of Fig 1.

Fig. 7. AnxaA5 gene knock down in the tenocytes, chondrocytes, and osteoblasts.

We performed qPCR and analyzed mRNA expression after AnxaA5 gene knock down (KD) in three representative cellular components of the enthesis, tenocytes (pTeno), chondrocytes (pCh), and osteoblasts (pOb) *in vitro*. We analyzed following mRNAs; *Anxa5* (A) , *Alp* (B), *Bmp4* (C), *Wnt5a* (D), *Ptc1* (E), *Ank* (F), *Enpp1*(G), and *Scx*, *Tnmd*, *Sox9*, *Runx2*, and *Opn* (H) . Y-axis shows fold change of expression relative to control . $*p < 0.05$.

Fig. 8. Schematic representation of the possible function of Anxa5 at the enthesis. Anxa5 is strongly expressed at the enthesis. Anxa5 prevents bone overgrowth at the enthesis, which depends on mechanical loading. *In vitro* experiments show that Anxa5 negatively regulates ALP expression, while it positively regulates ANK expression in tenocytes and chondrocytes, and ENPP1 in chondrocytes. Thus, it suggests that Anxa5 prevents bone overgrowth at the enthesis, whose formation is mediated through mechanical forces and modulating expression of pyrophosphate (PPi) regulators.

Supplemental Fig. 1. Comparison of body weight (**A**) and longitudinal tibial length (**B**) between Anxa5$^{+/+}$ (white bars), Anxa5$^{+/-}$ (gray bars), and Anxa5$^{-/-}$ (black bars) mice. Differences in body weight and tibial length at 4, 7, 16, and 40 weeks of ages in female and 40 weeks of ages in male mice were not significant (*t*-test). Data are the mean + SD.

Supplemental Fig. 2. Cross-sectional images used for measuring Ct.Pm.
Each cross-sectional image was obtained from μCT at the position as the distance (in mm) from the growth plate of the tibia. Cortical periosteal perimeter (Ct.Pm) in Fig. 2 was

measured in each cross-sectional image. Lines in sectional image and reconstructed 3D image of the upper panel indicate the positions at 0 and 3 mm distance from the growth plate.

Supplemental Fig. 3. Analysis of the tibial, femoral, and mandibular bones at 40 weeks of age.

(**A**) Representative view of microscopic images (upper), reconstructed μCT 3D images (middle), and cross-sectional images (lower) at insertion sites of tibial bone at 40 weeks of age in male mice. Images of tibia for Anxa5$^{+/+}$ (WT), Anxa5$^{+/-}$ (Het), and Anxa5$^{-/-}$ (KO) are shown. Bone ridge protrusions are indicated by arrowheads. Scale bar, 1 mm. (**B**) Representative view of microscopic images at insertion sites of femoral bone at 40 weeks of age in female Anxa5$^{+/+}$ (WT), and Anxa5$^{-/-}$ (KO) are shown (upper). Mean Ct.CSA of femoral bone measured by pQCT is shown (lower). (**C**) Representative view of reconstructed μCT 3D images and sagittal sectional images of mandibular bones in Anxa5$^{+/+}$ (WT) and Anxa5$^{-/-}$ (KO) female mice at 40 weeks of age. Lateral views of reconstructed 3D images and sagittal sections are shown. Specific protrusions at insertion sites of the digastric muscle to the bone in Anxa5$^{-/-}$ mice are indicated by arrowheads. B; mandibular bone, I; apical region of incisor, M1; first molar, M2; second molar. Scale bar; 1 mm.

Supplemental Fig. 4. (**A**) Schematic representation of tenotomy. The right patellar and tibialis anterior (TA) tendons of Anxa5$^{-/-}$ and Anxa5$^{+/+}$ mice at 12 weeks of age were severed. The left tibial bones were used as a normal control. At 8 weeks after tenotomy, tibiae were dissected and analyzed. (**B**) Changes in mean body weight from 12 to 20 weeks of age. Differences of body weight between Anxa5$^{-/-}$ (KO; straight line) and Anxa5$^{+/+}$ (WT; dotted line) mice were not significant.

Supplemental Fig. 5. TRAP activities at fibrocartilaginous enthesis. TRAP staining of transverse sections showing insertion sites of the soleus muscle to the tibial bone (Ti) in Anxa5$^{+/+}$ (WT; A) and Anxa5$^{-/-}$ (KO; B) mice at 40 weeks of age. Scale bars, 100 μm.

Table.1 Numbers of mice analyzed

	4w Female	7w Female	16w Female	40w Female	40w Male
Anxa5-/-	4	5	6	9	4
Anxa5+/-				4	7
Anxa5+/+	4	4	6	8	5

Table.2 Numbers of mice used for tenotomy and tail suspension

	tenotomy	Tail suspension	no suspension
Anxa5-/-	4	4	3
Anxa5+/+	5	4	3

Table.3 List of primer sequences used for RT-PCR analysis

	Accession number	Forward (5' to 3')	Reverse (5' to 3')
Gapdh	NM_001289726	GCCAAACGGGTCATCATCTC	GTCATGAGCCCTTCCACAAT
Alp	NM_007431	GATAACGAGATGCCACCAGA	AATGCTTGTGTCTGGGTTTA
Bmp4	NM_007554	CTCTTCAACCTCAGCAGCAT	GGTGTCCAGTAGTCGTGTGA
Wnt5a	NM_009524	CCTGCCTCGGGACTGGTTGT	CGGCCTGCTTCATTGTTGTG
Ptc1	NM_008957	CTCAGGCAATACGAAGCACA	GACAAGGAGCCAGAGTCCAG
Ank	NM_020332	ACGAGACAAGACCCTGGCATTAG	TGAAGATGGCACTAGAGCGAGAAG
Enpp1	NM_001308329	GGACGCTATGATTCCTTAGAGA	GCTGGTGAGCACAATGAAGA
Scx	NM_198885	CACCCAGCCCAAACAGATCTGCA	AGTGGCATCACCTCTTGGCTGCT
Tnmd	NM_022322	TCCCGCAAGTGAAGGTGGAGAAGA	AGTAAAGGTTCACAGACACGGCGG
Sox9	NM_011448	TCCTACAGCCCCTTCAACCT	GTGTCAGCGATGGGGGTGTA
Runx2	NM_009820	TTCCAGACCAGCAGCACTCC	CTTCCGTCAGCGTCAACACC
Opn	NM_001204233	CAGGAGAGTGCCGATCAGTC	GGAACTGTGTTTTTGCCTCT

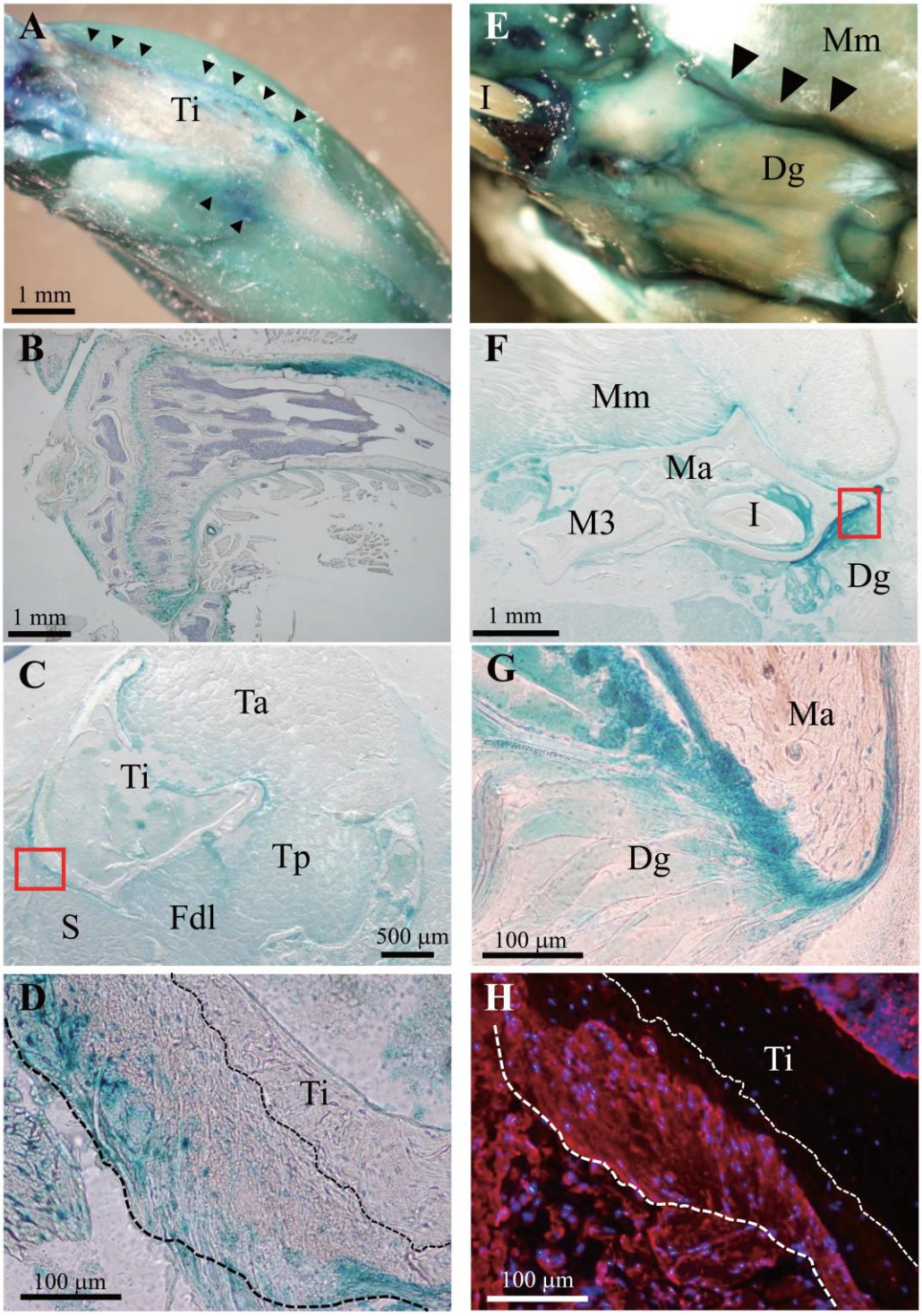

Fig. 1 Shimada et al. JBMR

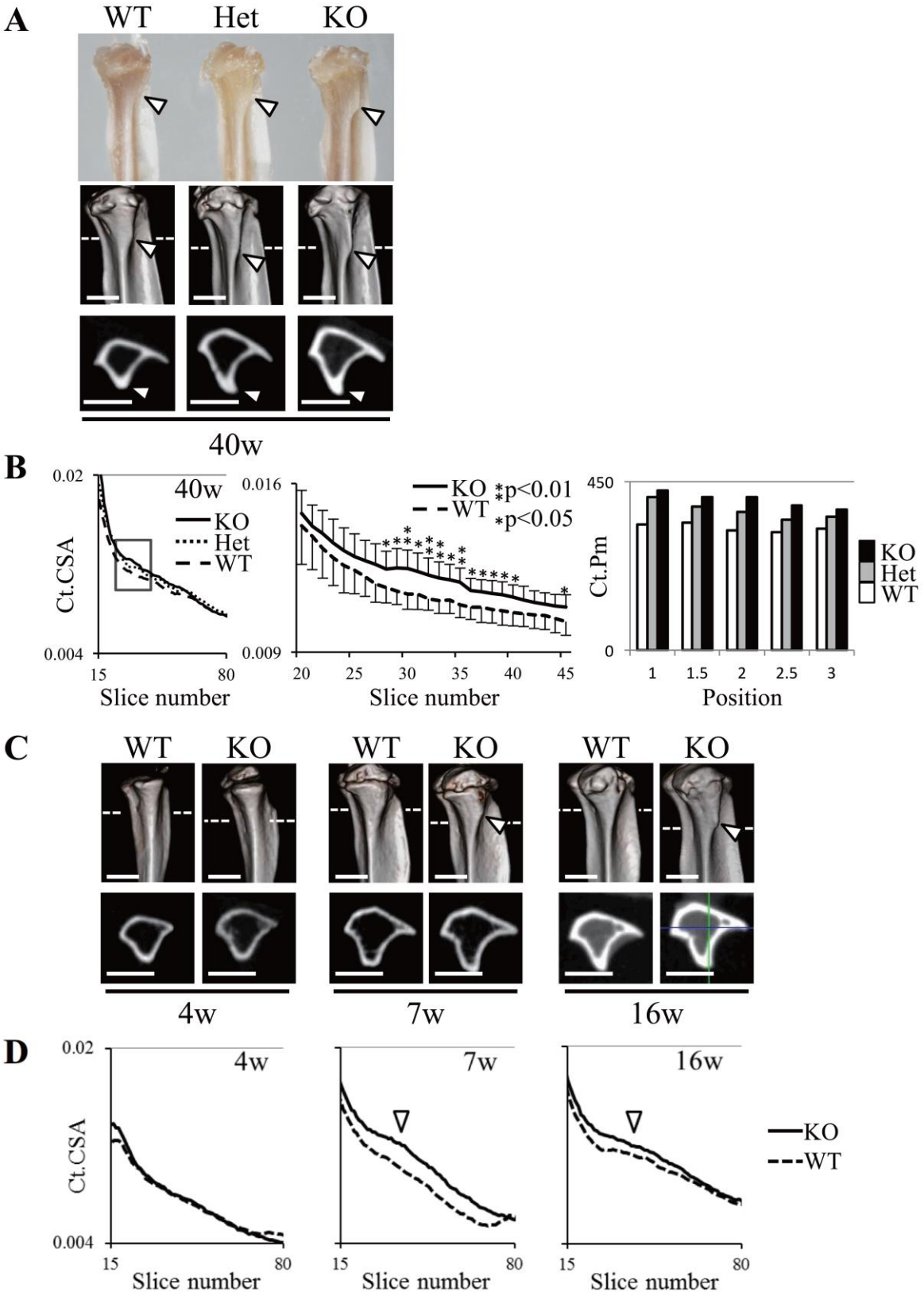

Fig. 2 Shimada et al. JBMR

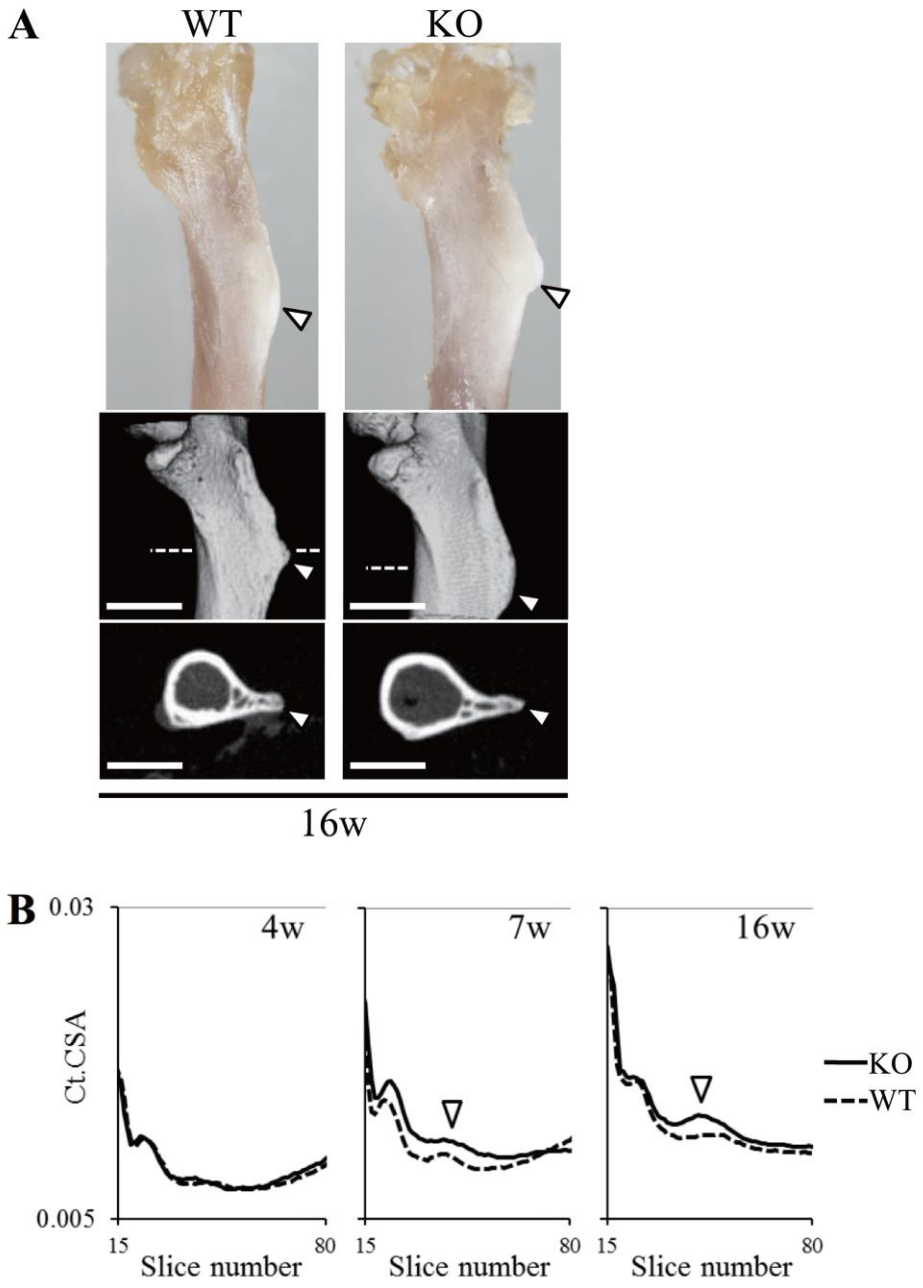

Fig. 3 Shimada et al. JBMR

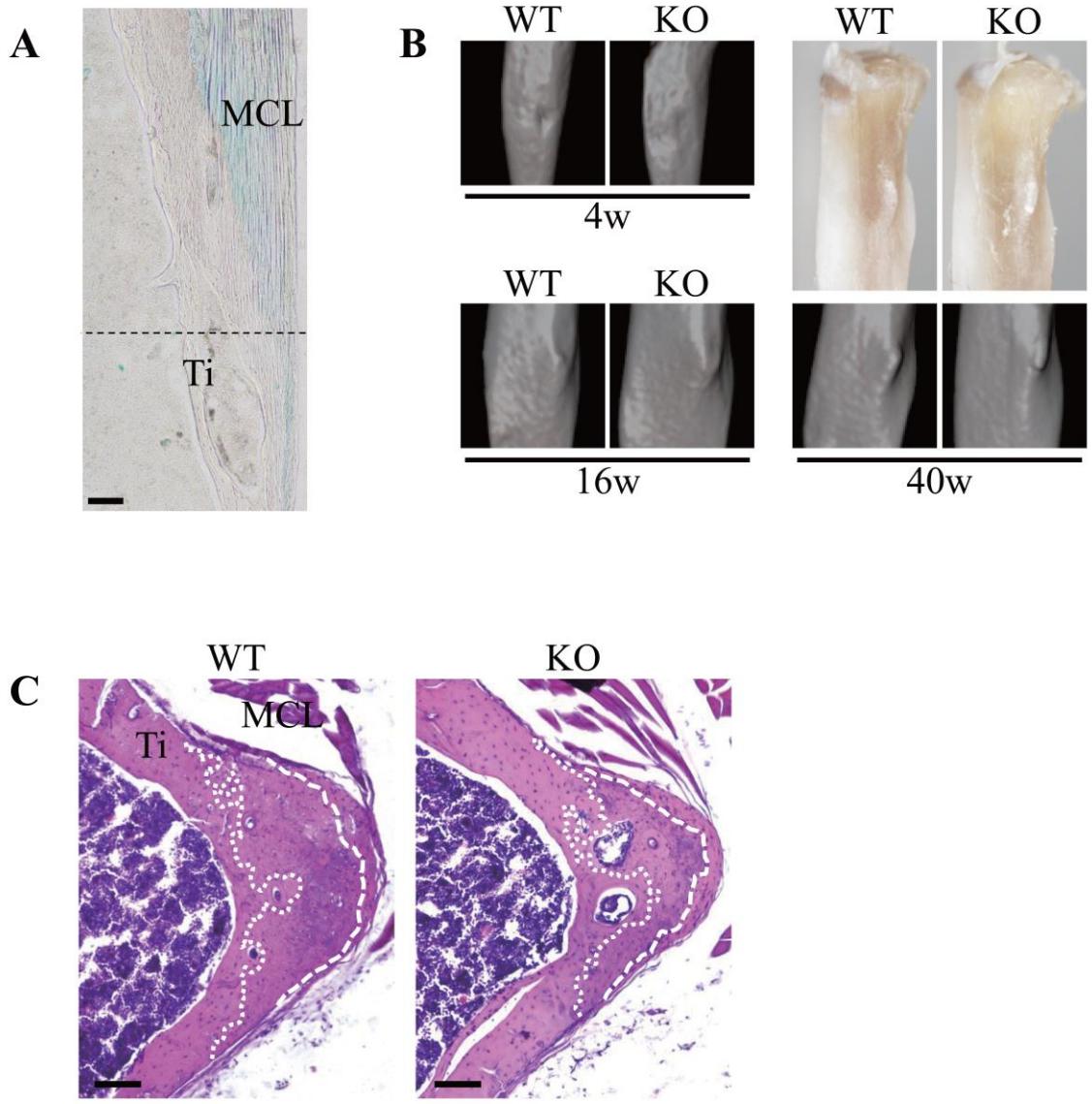

Fig. 4 Shimada et al. JBMR

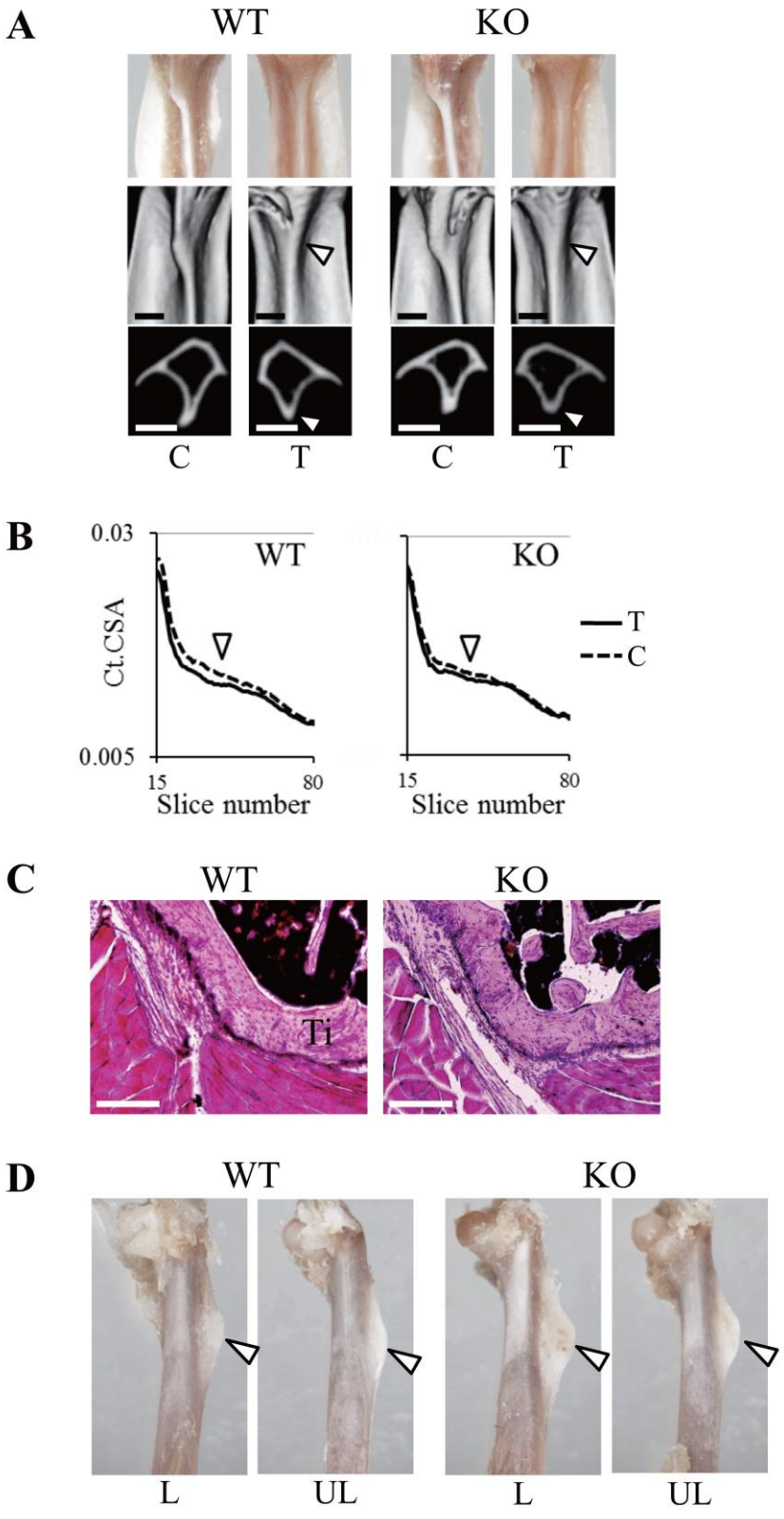

Fig. 5 Shimada et al. JBMR

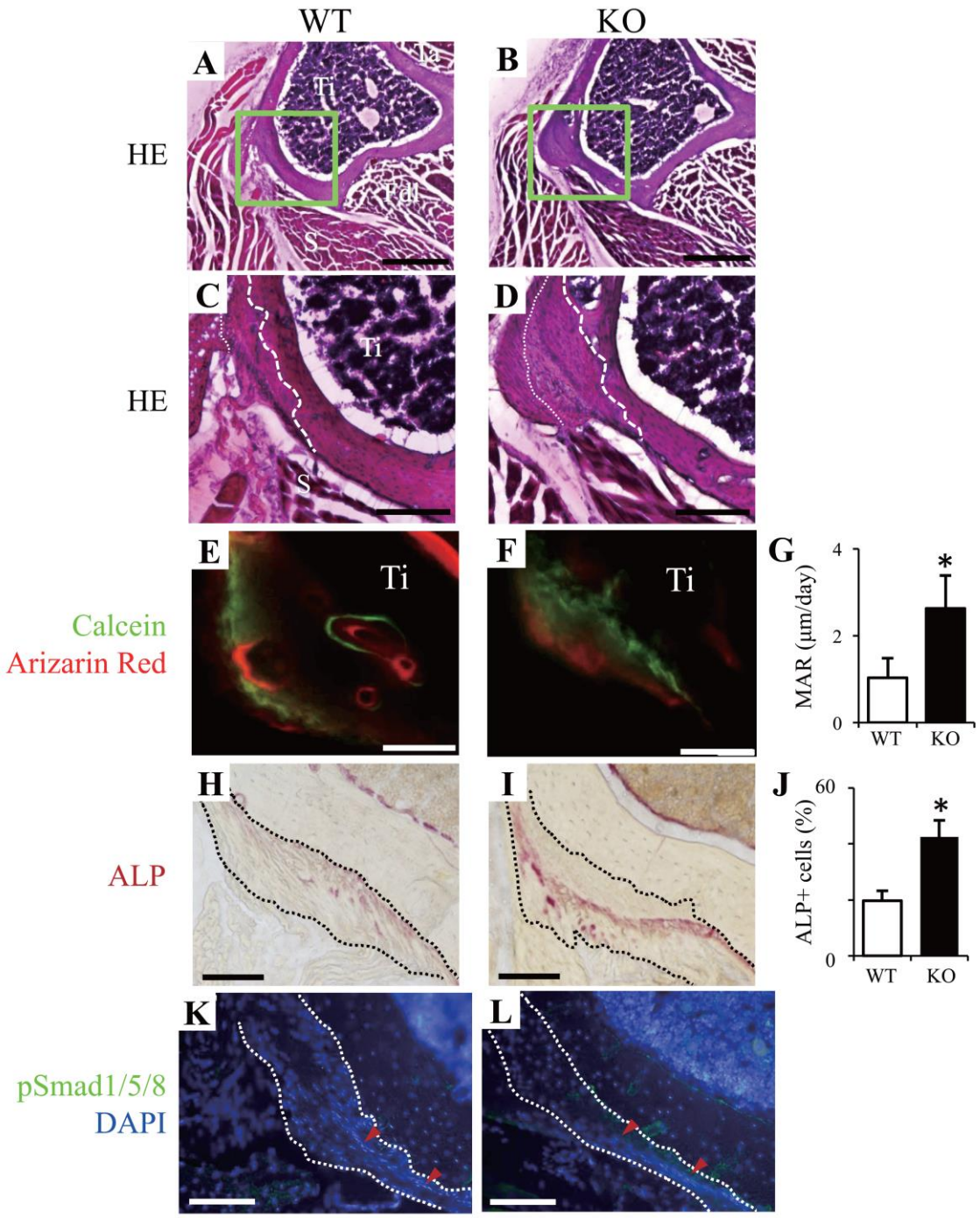

Fig. 6 Shimada et al. JBMR

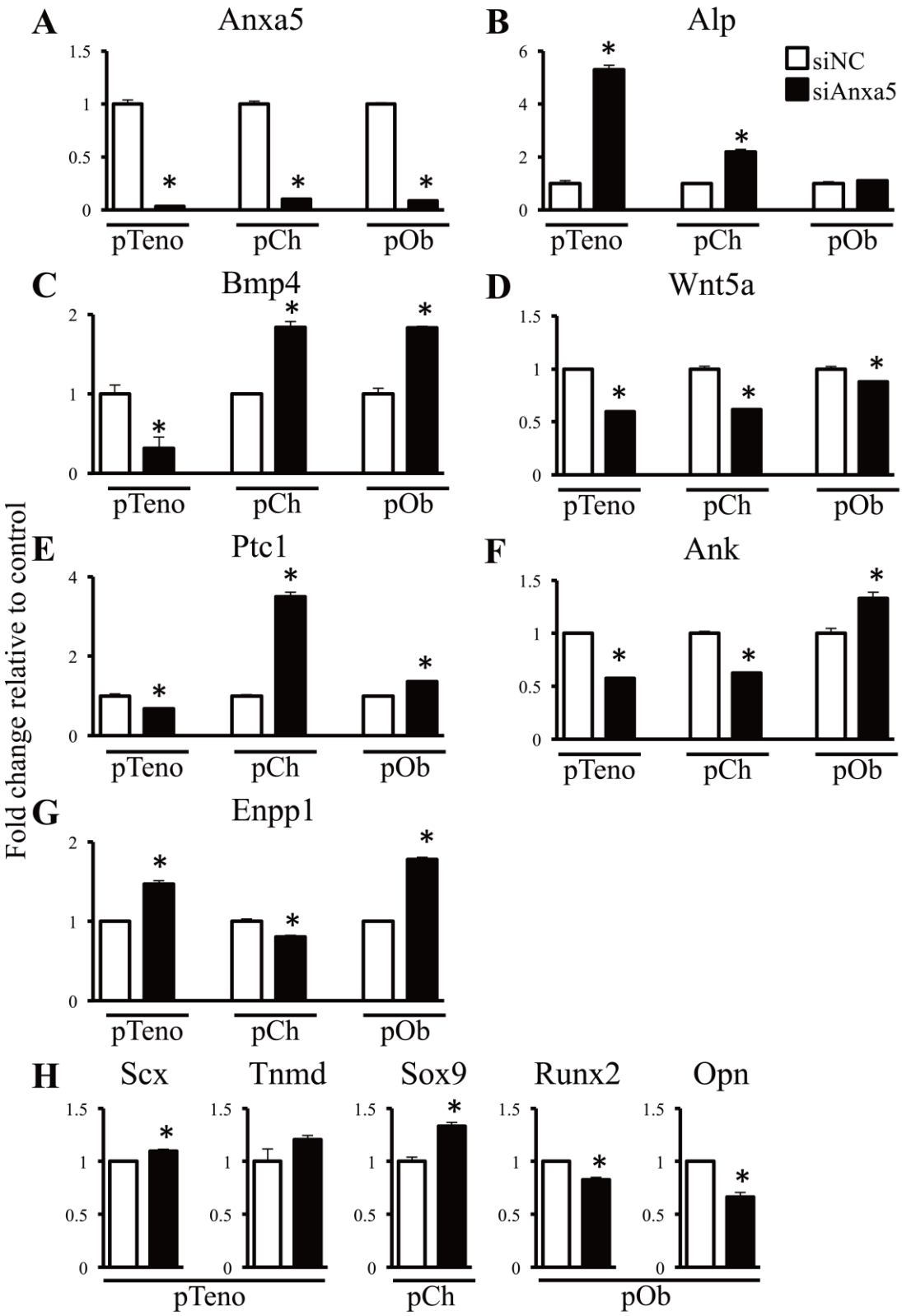

Fig. 7 Shimada et al. JBMR

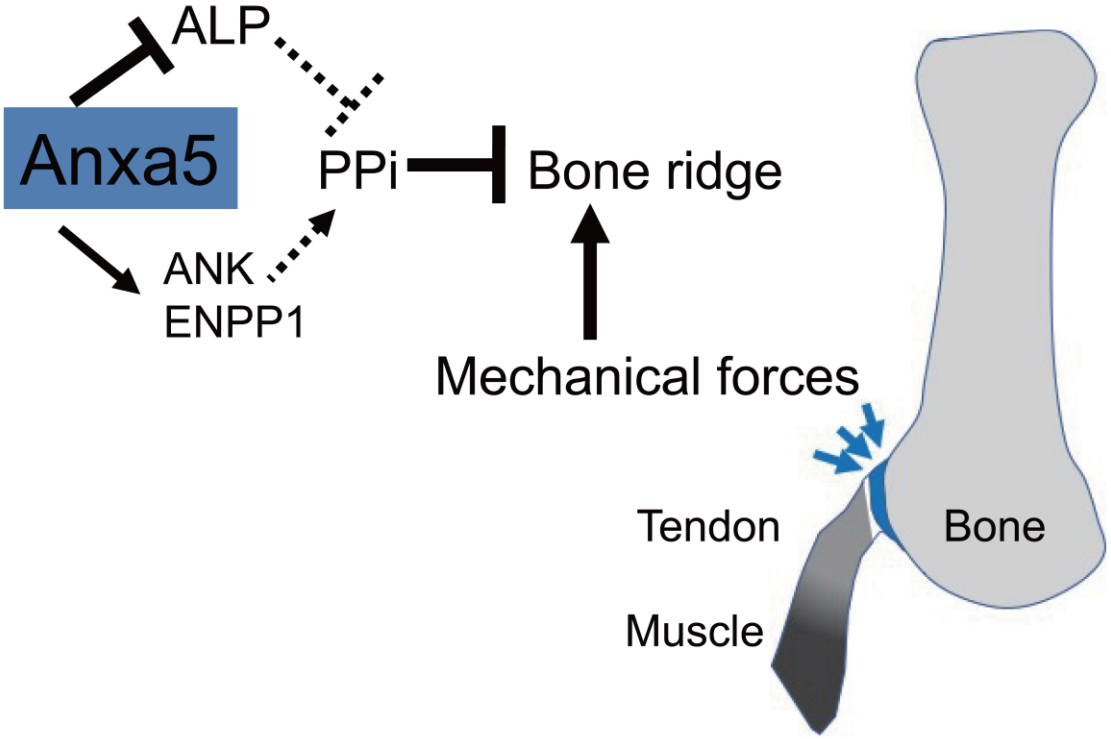

Fig. 8 Shimada et al. JBMR